PHYSICAL CHEMISTRY
OF SURFACE PHENOMENA

Tuning Optical Character of ZnO Thin Films with Ag Doping by Different Synthetic Routes

Sadia Shahbaz[a], Muhammad Saifullah Awan[b], Saleem Akhtar[c], Afzal Hussain[d], and Safeer Ahmed[a,*]

[a] *Department of Chemistry Quaid-i-Azam University, Islamabad, 45320 Pakistan*
[b] *Nanoscience and Technology Department, National Centre for Physics, Quaid-i-Azam University, Islamabad, 45320 Pakistan*
[c] *IbniSina Institute of Technology, H-11, Islamabad, Pakistan*
[d] *Pakistan Council of Renewable Energy Technologies, H-9/1, Islamabad, Pakistan*
* e-mail: safeerad@qau.edu.pk

Abstract—Silver (Ag) doped zinc oxide (ZnO) thin films are synthesized through three different methods namely sol–gel deposition, electrodeposition, and chemical bath deposition (CBD) on conducting glass substrate. The XRD patterns of ZnO and Ag/ZnO visibly revealed the presence of hexagonal wurtzite polycrystalline structure with the films oriented along the (101) plane. The shift in peak position with silver doping provided a strong evidence of Ag^+ substitution for the Zn^{2+} site. The crystal structure, surface morphology and the particle size distribution were monitored for the 0.5 to 4 wt % Ag content. The SEM analysis evidently showed the effect of Ag^+ doping whereby a highly porous structure was obtained for the CBD films and a layered structure for the sol–gel and electrodeposition films. The UV–Vis transmittance and absorbance spectra showed highest transmittance in sol–gel films which further increased on Ag^+ addition and a decrease in transmittance was observed in electrodeposited and CBD films. The higher absorbance and longer absorption window (up to 900 nm) were recorded in CBD and electrodeposition films than to that of sol–gel films. Lowering in band gap of the CBD films (up to 1.98 eV), a slight decrease in electrodeposited films (3.12 eV) and nearly no change in the sol–gel films (3.20 eV) was recoded upon silver doping.

INTRODUCTION

ZnO is a wide band gap *n*-type binary compound of Group II–VI that usually crystallizes into hexagonal wurtzite or the zinc blende where the former phase is more stable under ambient conditions [1, 2]. The uniqueness lies in its wide band gap properties and large exciton binding energies of nearly 60 MeV. It has found its applications in pH sensors, varistors, surface acoustic wave devices, optical wave guides, biosensors and in photovoltaics [3, 4]. It is used as the transport layer in dye sensitized solar cells (DSCs) in the form of thin films and is second most important semiconductor after TiO_2. The composition, morphology and the thickness of the semiconductor are critical parameters that determine the desired character of a thin film in optical and electrical applications. Many methods are known to fabricate ZnO thin films on transparent conductive oxide substrates including sol–gel deposition, chemical vapor deposition (CVD), molecular beam epitaxy (MBE), chemical bath deposition (CBD), electrodeposition (ECD), spray pyrolysis, pulsed laser deposition (PLD), etc. [5–8]. The sol–gel, electrochemical and chemical bath deposition methods offer

low production cost, ease of fabrication, facile doping at molecular level, control composition and manageable deposition equipment. All this make them more suitable for large scale production of thin films.

The sol–gel deposition process confers the formation of oxide network through molecular precursors in the liquid medium that results in the formation of the homogeneous films with unique optical, electrical, thermal, and resistive properties [6]. The electrodeposition method is a surface deposition method that results in the deposition of the adherent layer of one metal over the other due to the reduction of ions from the aqueous, organic and the fused electrolytes [7, 9]. On the other hand, chemical bath deposition is a technique that involves the controlled precipitation of the compounds, low temperature processing, controlled pH resulting in the formation of good deposits on the suitable substrates. CBD being complementary to CVD includes two types of nucleation namely heterogeneous and homogeneous accompanying the processes such as mass transport, adsorption, diffusion, desorption, and growth [10].

To produce novelties and modifications in terms of electrical, optical and structural properties in the host atoms, doping is considered as a feasible approach which can be characterized as either *n*-type or *p*-type. The *n*-type doping is mostly achieved through group II-A, III-A, and IV-A elements whereas *p*-type doping, ordinarily difficult, is achieved through group IA, VA, and IB elements [11]. Ag is thought to be an amphoteric metal that can behave as either *p*-type or *n*-type dopant with the variation in the concentration. Silver is mostly considered as an electron sink and covers a wide range of potential applications particularly photocatalytic, photovoltaic, photo luminescent etc. [3, 5, 12]. As a result, it permits electron transfer from ZnO to Ag across the interface when incorporated with ZnO which also facilitates the photogenerated electron hole pair separation [13]. It is usually observed that the noble elements doped semiconductors are very effective in enhancing the visible light absorption and reducing the back reaction thus increasing the efficiency of the photovoltaic devices [14, 15]. Recently, Xu et al. reported the annealing time strongly influences the optoelectronic properties of Ag-doped ZnO films [16]. Similarly, in another report a detailed account of electrical and optical properties is reported while varying amount of Ag ions as dopant [17]. The effect of silver doping on the optical and electrical properties of ZnO have also been proven by green synthesis method [18]. Considering its role as a useful extrinsic impurity several investigations on the doped ZnO have been performed w.r.t. applications such as semiconductors, solar cells, optoelectronic devices [19−23]. However, as silver belongs to noble family, it is usually unstable and may oxidize when exposed to air [13]. In this work, ZnO and Ag/ZnO thin films have been synthesized through three different methods which includes sol−gel deposition, electrodeposition, and chemical bath deposition. A comparison among the thin films is made on the account of morphological and optical properties while discussing the role of synthesis method. The effect of Ag^+ doping is particularly discussed for varied compositions of the dopant. Another important aspect of the studies is the mechanistic approach to relate the morphological attributes to optical and electrical properties of the developed thin films.

EXPERIMENTAL

The procedure for preparing the various ZnO and Ag/ZnO thin films through different methods is given below.

Preparation of Sol−Gel Deposited ZnO and Ag−ZnO Thin Films

The films deposited throughsol-gel method were synthesized as described by Cui et al. [24] by dissolving 0.5 M solution of high purity (≥99%) zinc acetate dihydrate $Zn(CH_3COO)_2·2H_2O$ (precursor) and silver nitrate $Ag(NO)_3$ (>90% dopant) in butanol (>99% solvent) having milky color. The monoethanol amine was (>95%) added as a stabilizer in a 1 : 1 ratio to obtain a colorless solution. The resulting mixture was stirred for 2 h at 65°C to obtain a clear and homogeneous solution which was then aged for about 24 h [25]. The ZnO thin films were fabricated by dipping the FTO substrates which are 3.15 mm in thickness and 15 Ω/cm² resistance in the above aged solution for about 5 min and then dried at 300°C. The procedure from dipping to drying is repeated for at least 2−3 times followed by annealing in a box furnace for ∼30 min at 600°C [6, 26]. The whole process is repeated for Ag doping as well with the addition of $Ag(NO_3)_2$ to the main solution.

Preparation of Electrodeposited ZnO and Ag−ZnO Thin Films

For electrodeposition of the films, the deposition was carried in aqueous solution containing 0.1 M zinc nitrate hexahydrate $(Zn(NO_3)_2)·6H_2O$ (>99%) and silver nitrate $Ag(NO)_3$, 0.1 M potassium nitrate (KNO_3) (95%) as the supporting electrolyte and 4 g/dm³ of (PVP) as a stabilizing agent in the electrochemical cell. Three electrode assembly namely Ag/AgCl as a reference, platinum as a counter and a piece of FTO (substrate) as a working electrode was used. The electrochemical bath temperature was maintained at 60°C with constant stirring [7, 27]. The deposition of ZnO and Ag/ZnO thin films on FTO substrate took place at −1.1 V vs. Ag/AgCl for about 10 min. The resultant thin film of $Zn(OH)_2$ was whitish in color. The electrodeposited film was rinsed with distilled water and annealed at 380°C for 40 min in a muffled furnace to get ZnO thin films.

Preparation of Chemical Bath Deposited ZnO and Ag−ZnO Thin Films

The ZnO and Ag/ZnO thin films deposited through the chemical bath deposition method have been synthesized through the method developed by Abdullah et al. [28]. An aqueous solution of 0.05 M zinc nitrate hexahydrate $Zn(NO_3)_2·6H_2O$, silver nitrate $Ag(NO)_3$, and 1.0 M solution of urea $CO(NH_2)_2$ (>99%) were thoroughly mixed. The pH of the solution was maintained at 4, while continuous stirring was done during the addition of nitric acid. The temperature of the bath was kept at 60°C with the FTO glass inserted in the solution. The whole deposition process was done for 24 h at 60°C with constant stirring. The resultant films were thoroughly washed with distilled water and dried at 50°C in an oven and annealed at 380°C for 40 min in a box furnace. After developing the thin films the coated FTOs were kept in a desiccator for further studies. The proposed mecha-
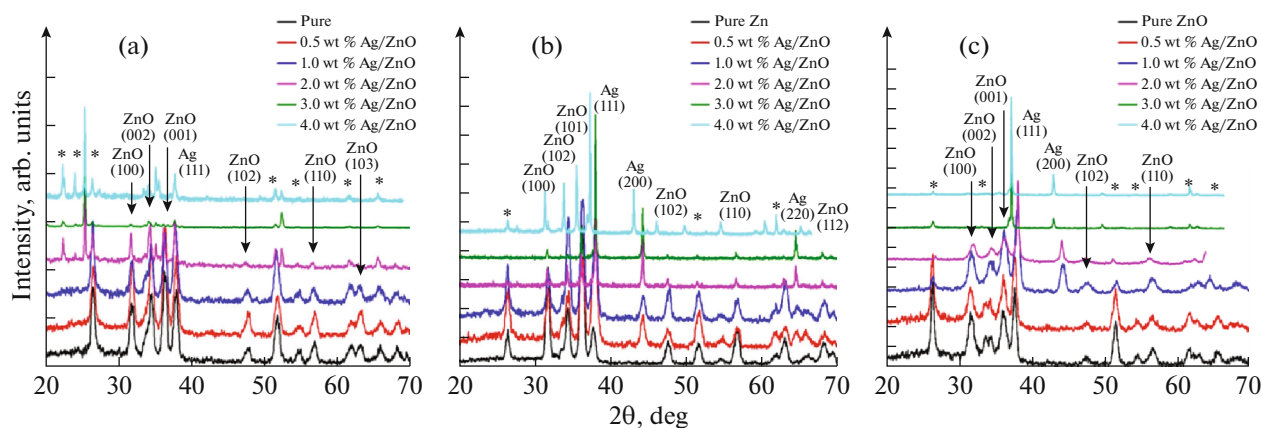
Fig. 1. XRD pattern of ZnO and $Zn_{1-x}Ag_xO$ than films by (a) sol−gel deposition method, (b) electrodeposition method, and (c) chemical bath deposition method.

nisms according to the Scheme 1−3 are mentioned below.

Structural analysis was carried out to determine the phase formation, morphology, and the chemical composition of the thin films. The crystal structure was identified through XRD analysis employing Panalytical 3040/60 X'pert PRO diffractometer using CuK_α source at 45 kV and 40 mA and the peaks were recorded between 30° to 70° with the scan rate of 0.04° and step time of 1s/step. The microstructural analysis of ZnO and Ag/ZnO thin films on the FTO substrate was performed using scanning electron microscopy (SEM) Quanta 600F. To determine the transmittance and absorbance spectra of the deposited samples, a double beam UV−Vis−NIR specord 200 spectrophotometer was used using software Aspect plus version 7.0.

RESULTS AND DISCUSSION

X-ray Diffraction Studies

The XRD patterns of the ZnO and Ag/ZnO thin films through different methods covering the 2θ range of 20°−70° have been shown in the Fig. 1. These X-ray diffractograms were used to analyze the crystallite size and phase identification of ZnO and $Zn_{1-x}Ag_xO$ thin films on FTO substrate. The XRD patterns are in good consistency with the standard JCPDS card nos. 00-005-0664 and 00-001-1164 for ZnO and Ag, respectively. The diffraction peaks corresponding to (100), (002), (101), (102), and (112) corresponds to ZnO, whereas the asterisk indicates the FTO substrate. The obtained patterns showed the presence of polycrystalline hexagonal wurtzite phase with the (101) peak of ZnO being the most intense one as compared to others [6, 29].

From Fig. 1a, it is apparent that the crystal structure for the deposited films through sol−gel, electrodeposition and chemical bath is oriented along (101) plane and the peak intensity of (101) plane including other peaks decreased as the silver content is increased. For sol−gel deposited film, the decrease is more prominent for higher silver content. On the other hand, the peaks became sharper with the increase in silver content indicating the increase in the crystallite size. In addition, the 2θ values corresponding to (101) peak shifted towards the lower angles due to compressive strains, increased lattice mismatch and large differences in ionic radii between Ag^+ and Zn^{2+}. These results are in strong agreement that Ag particles have been located on the ZnO surface. In case of electrodeposition and chemical bath deposited films, (Figs. 1b, 1c) a strong doping attributed behavior was observed with the appearance of additional peaks corresponding to (111) and (200) planes for only a small amount of dopant (at ≤1%) that became more intense as the silver content is increased. Tarwalet al. also mentioned the appearance of Ag peaks in the Ag/ZnO films with the shift toward the lower angle [30] as compared towards the higher angle as mentioned by Winkler for Mg doping [31]. No marked shift in peak position has been observed for lower dopant addition which indicated that the silver atoms are positioned on the host crystal structure and eliminated the possibility of their presence in the crystal structure or substituting the Zn site. However, for chemical bath deposited films, the (101) peak of ZnO suppressed in intensity as compared to silver (111) peak with the increase in the dopant concentration that is an indication of the increased structural distortion and large variation in the lattice parameters that resulted from the substitution of larger silver ions (122 pm) for smaller zinc ions 72 pm [32].

In view of the particle size, the films deposited from all the three methods showed an increase in the crystallite size as the silver content is increased. This increase was very large, nearly doubled, in the chemical bath deposited films as compared to the others when doped for 0.5 to 2 wt % of Ag. However, for higher content of Ag (<2%) there was a decrease in crystallite size in contrast to sol−gel, in electrodeposi-
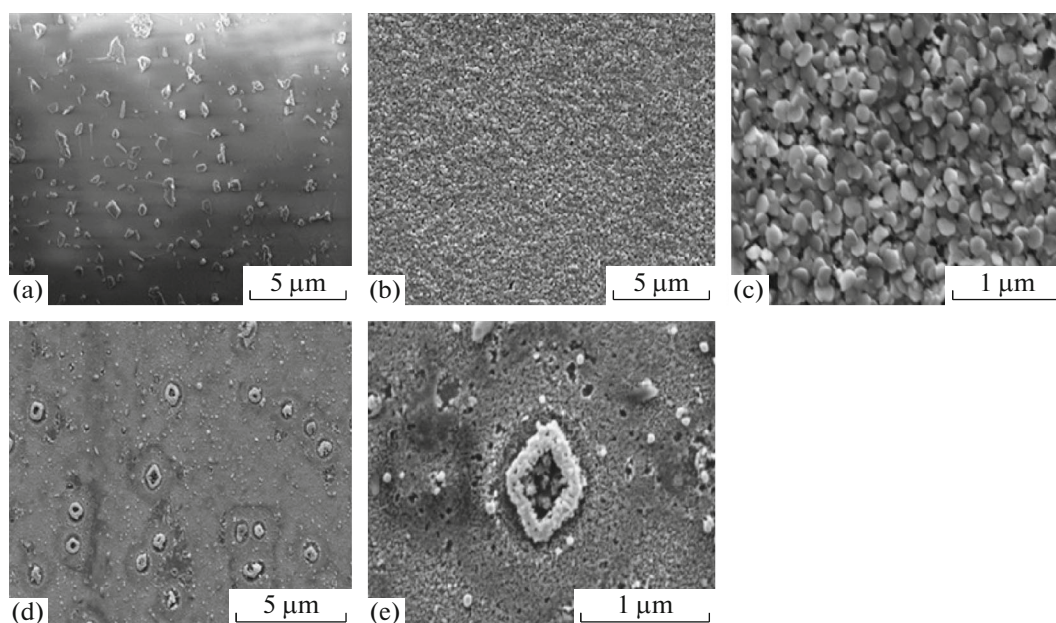
Fig. 2. SEM images of ZnO and $Zn_{1-x}Ag_xO$ thin films on FTO substrate by sol−gel deposition method (a) pure ZnO, (b, c) 1 wt % $Zn_{1-x}Ag_xO$, and (d, e) 4.0 wt % $Zn_{1-x}Ag_xO$ at low and high magnification, respectively.

tion methods where a continuous increase in crystallite size was recorded.

Scanning Electron Microscopic Studies

The scanning electron microscopic (SEM) images of sol−gel, electrochemical and chemical bath deposited samples under low and high magnifications have been shown in Figs. 2−4. The SEM micrographs (Fig. 2a) of the sol−gel deposited ZnO thin films on FTO substrate show the effect of ageing period of 24 h. The micrographs showed some irregular shaped (0.38 μm) and homogeneous particle distribution. However, the particle density can be increased by increasing the number of coatings on the FTO substrate. These discrete particles may evolve into more regular shaped morphologies oriented along (101) plane direction upon increasing the film thickness. The 1 wt % Ag/ZnO thin films formed through sol−gel showed somewhat regular and uniform distribution of pellet type structures (Figs. 2b, 2c). The 4 wt % Ag/ZnO (Figs. 2d, 2e) showed the uniform aggregation of micro sized particles (0.57 μm) with the shift in morphology from irregular to highly regular porous core-shell type structures with the increase in aggregation level having a porous disc like morphology as compared to that of pure ZnO thin films. It is also observed that the particle size also increases as the percent of silver content is increased in the ZnO thin films.

The SEM micrographs of the electrochemically deposited pure ZnO thin film on FTO substrate at −1.1 V potential indicated the formation of hierarchal

sort of porous irregular shaped structures with uniform distribution on the substrate (Fig. 3a). These micro sized particles (0.23 μm) were seen to form aggregates as well as hexagonal shaped enlarged structures of ZnO at certain locus of the substrates. The 1 wt % Ag/ZnO thin film (Figs. 3b, 3c) showed the highly porous interconnected layered structure containing nanoparticles above the pool of the micro sized disc like and hexagonal protruded shaped particles (0.3 μm) of Zn and Ag. These were transformed into some regular hexagonal and globular large sized interconnected micro (1.8 μm) structures for 4 wt % Ag/ZnO (Figs. 3d, 3e) above which there lied the porous layered structures (0.2 μm). The size and compactness of the lower layered particles has also increased as compared to that of the 1 wt % Ag/ZnO thin film.

The chemical bath deposited films indicated the formation of the micro porous interconnected network (1.2 μm) (Fig. 4a) along with the scattered rods at various positions on the FTO substrate. The 1 wt % Ag/ZnO thin films (Figs. 4b, 4c) showed the uniform distribution of scattered nano-rods and beads like spherical structures. Whereas, an increased density of the aggregated rods and spherical shaped enlarged particles (0.12 μm) were observed for the 4 wt % Ag/ZnO thin films on the FTO substrate (Figs. 4d, 4e) along with the formation of large sized porous chunks at various positions containing high Ag content as compared to Zn. In contrast to the films deposited through the other two methods, the chemical bath deposited films showed two important differences. The first is the formation of highly porous and well-fixed entangled rope like structure for pure ZnO. The
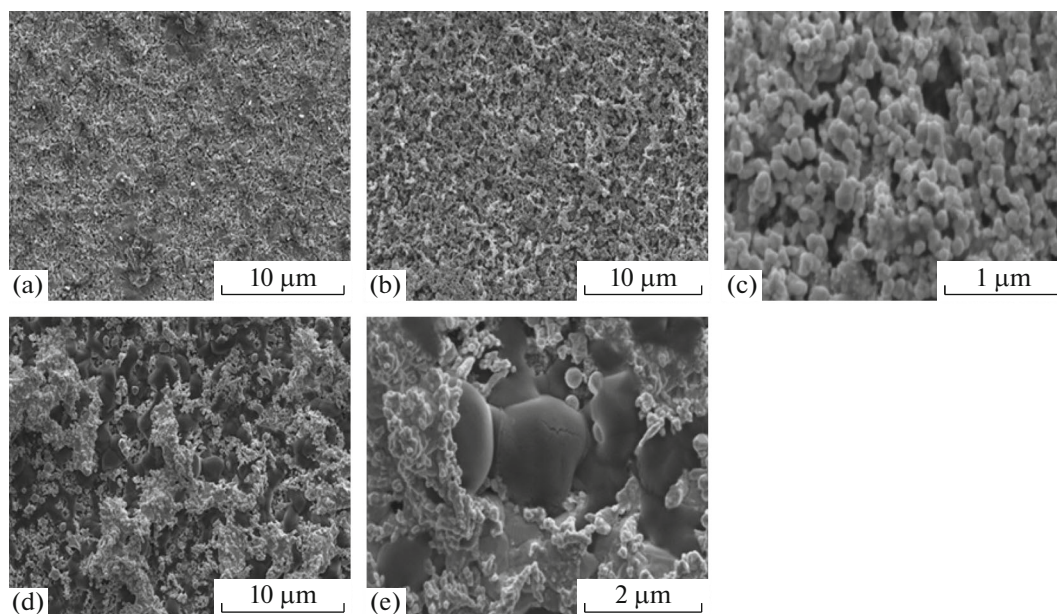
Fig. 3. SEM images of ZnO and $Zn_{1-x}Ag_xO$ thin films on FTO substrate by electrodeposition method (a) pure ZnO, (b, c) 1 wt % $Zn_{1-x}Ag_xO$, and (d, e) 4.0 wt % $Zn_{1-x}Ag_xO$ at low and high magnification, respectively.
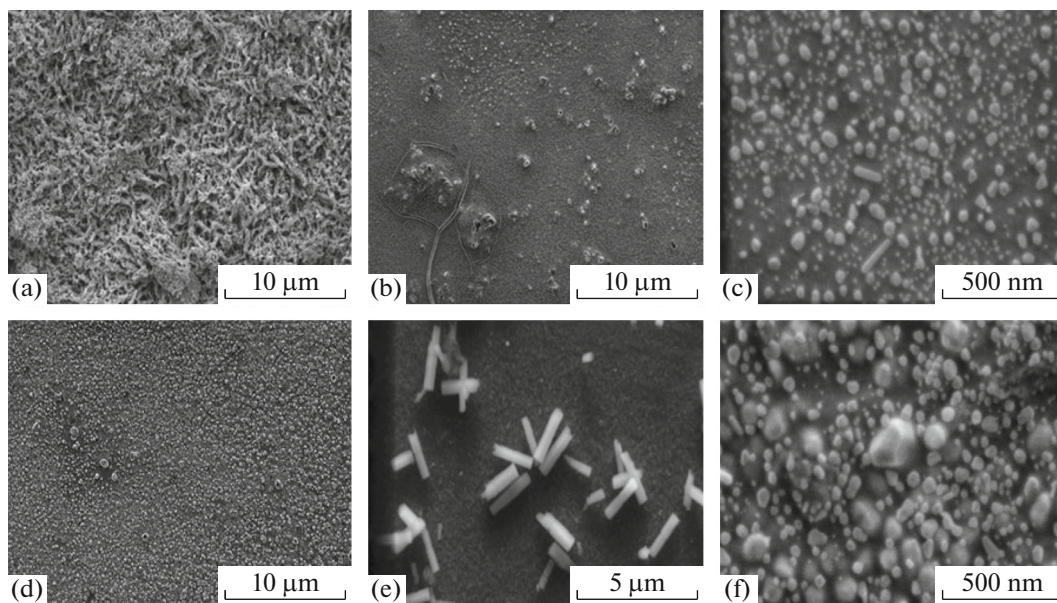

Fig. 4. SEM images of $Zn_{1-x}Ag_xO$ thin films on FTO substrate by chemical bath deposition method (a) pure ZnO, (b, c) 1 wt % $Zn_{1-x}Ag_xO$, and (d–f) 4.0 wt % $Zn_{1-x}Ag_xO$ at low and high magnification, respectively.

second is the effect of adding Ag which turned the porosity into filled and compact structures either of spherical shaped at low content of Ag and rectangular shaped large sized compact structures at higher Ag content.

Based on the results obtained as deliberated above the sol−gel deposited films showed less compact and more discrete patterns as compared to the films obtained through the chemical bath and electrodeposition methods. Here the 1 wt % Ag doped ZnO thin films showed more homogeneity with the reduced particle size as compared to that of pure and 4 wt % Ag doped ZnO thin films. The formation of the homogeneous and interconnected double layered structures were observed in the films through electrodeposition approach which indicated the effect of applied potential that served to form more interconnected structures as compared to the sol−gel procedure. The later method relied on the repeated dip coating and drying

practices and thus left discrete structures which became more isolated at 4 wt % Ag doping. The structures obtained through chemical bath deposition method also showed porous regions over the substrate surface with the restriction of the aggregation level at some specific points. The particle sizes also get affected with the addition of small amount of silver as a dopant in the acidic pH range.

Optical Studies

The absorption spectra clearly showed band edge at 381 nm (3.21 eV) (Figs. 5a, 5c, 5e) for the thin films deposited on FTO substrate with different silver content. The transmittance spectra in the (Figs. 5b, 5d, 5f) revealed that the films synthesized (pure ZnO and silver doped) by all the three methods experienced a decrease in the transmittance value in the UV range when compared to the FTO substrate. Some abnormal behavior was observed for sol−gel deposited samples as maximum transmittance is assigned to 4.0, 3.0, and 2.0 wt % silver contents as compared to the electrodeposited films where 2.0 wt % Ag−ZnO film has the lowest transmittance values. The films deposited by chemical bath deposition method showed unusual decrease in transmittance for the UV region which gradually increased up to 25% in the visible region as compared to the sol−gel and the electrochemical methods. The transmittance spectra are indicative of light interference effects at the interface of substrate material and the thin film. The decrease in the transmittance values for pure, 0.5, 1.0, and 2.0 wt % silver doped ZnO in the visible region is due to the grain boundary and surface scattering effects. Moreover, this decrease has been observed due to the light absorption by surface plasmon resonance effects in the visible region a usual property of metal nanoparticles.
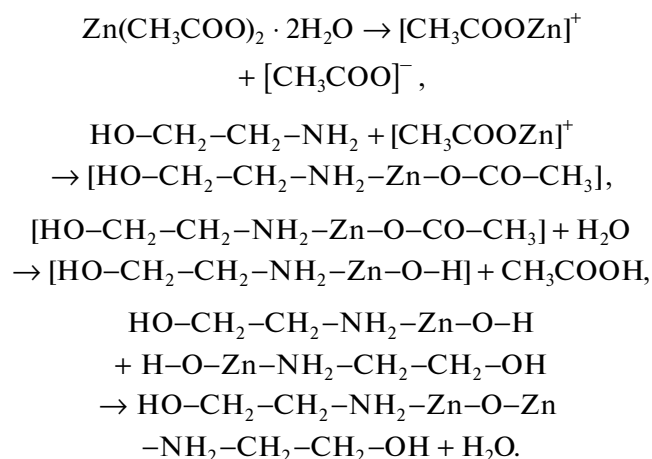
From Fig. 5a the maximum absorbance at 368 nm is observed for 0.5 wt % silver doped ZnO whereby a decrease was observed for higher silver content 4.0 wt % 358 nm. The sharp excitonic peak for 0.5 wt % Ag^+ indicated the small size distribution of nanoparticles whereas the broad peaks are indicating the increase in the crystal size. An increase in absorbance towards the higher wavelength side (visible region) indicated the role of silver particles that are dispersed in the ZnO and lie on its surface resulting an increase in the surface area of the Ag doped ZnO thin films. The band gap values also decrease with the increase in the silver content while it is 3.25 eV for the pure ZnO and for the FTO, it corresponds to the 4.1 eV (see supporting information, Fig. S1 (see Supplementary Information)). The absorption edge also shifted to the higher wavelength region and the band gap narrowing ascribed to the Ag^+ substitution for the Zn^{2+} site. For the films deposited through electrodeposition, the films possess low transmittance in the UV region with the absorption edges of the doped films shifted towards the higher wavelength region as com-

pared to pure ZnO thin film. The transmittance values increased in the visible region with the maximum transmittance for the pure ZnO and decreased with the increase in the silver content. An exception is the 2.0 wt % film which showed lowest transmittance in the visible region probably due to the increased surface and grain boundary scatterings.

The maximum absorbance was observed at 369 nm for all the films and the absorption edge was observed to be shifted to the higher wavelength resulting in the narrowing of the band gaps. A decrease in the band gap was observed for all samples and the values are enlisted in the (Table S1) and similar observations are reported previously [33, 34]. The shifting of absorption edges to the higher wavelength regions is an indicative of rough and irregular grain boundaries that resulted in the increased surface and grain boundary scattering effects whereas the band gap narrowing showed the Ag^+ substitution for the Zn^{2+} site. A marked decrease in band gaps was observed for the chemical bath deposition.

Mechanism of Ag−ZnO Film Formation

Mechanism of sol−gel deposited ZnO and Ag−ZnO thin films. From the proposed mechanisms [35] (Scheme 1), it has been observed that, monoethanol amine (a weak base) has been used to hamper the Zn^{2+} condensation and to enhance the solution`s pH. The CH_3COOH group from the precursor and the bidentate ligand acted as the chelating agents. The mono-acetate specie formed forms a complex with monoethanol amine meanwhile the OH^- species formed during the initial stage of constrained hydrolysis formed small oxo species while progressive condensation resulted in the formation of colloids and precipitates. The oligomers formed during the hydrolysis and polycondensation were easily transformed into ZnO species when annealed at a temperature higher than 350°C [2, 35] (Scheme 1).

$$Zn(CH_3COO)_2 \cdot 2H_2O \rightarrow [CH_3COOZn]^+$$
$$+ [CH_3COO]^-,$$

$$HO-CH_2-CH_2-NH_2 + [CH_3COOZn]^+$$
$$\rightarrow [HO-CH_2-CH_2-NH_2-Zn-O-CO-CH_3],$$

$$[HO-CH_2-CH_2-NH_2-Zn-O-CO-CH_3] + H_2O$$
$$\rightarrow [HO-CH_2-CH_2-NH_2-Zn-O-H] + CH_3COOH,$$

$$HO-CH_2-CH_2-NH_2-Zn-O-H$$
$$+ H-O-Zn-NH_2-CH_2-CH_2-OH$$
$$\rightarrow HO-CH_2-CH_2-NH_2-Zn-O-Zn$$
$$-NH_2-CH_2-CH_2-OH + H_2O.$$

Scheme 1. Schematic representation of ZnO and $Zn_{1-x}Ag_xO$ thin film synthesis by sol−gel deposition method on the FTO substrate.
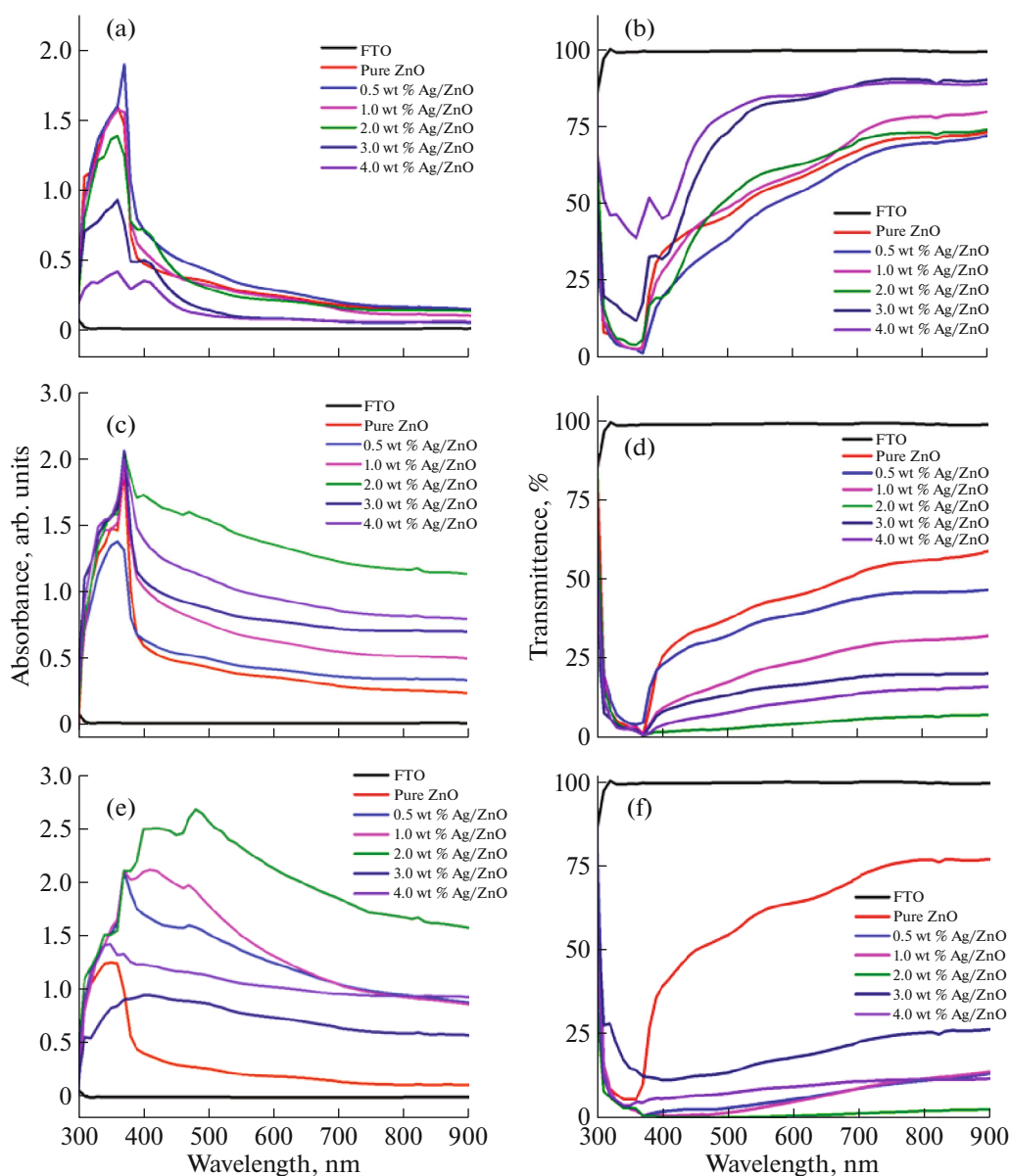
Fig. 5. Absorbance and transmittance spectra of ZnO and $Zn_{1-x}Ag_xO$ thin films on FTO substrate by (a, b) sol−gel deposition method, (c, d) electrodeposotion method, and (e, f) chemical bath deposition method, respectively.

Mechanism of Electrodeposited ZnO and Ag−ZnO Thin Films

The proposed mechanism (Scheme 2) for the electrodeposition method suggested [19, 36, 37] that hydroxyl ions generated in the first step react with the zinc ions to yield $Zn(OH)_2$ which then decomposes to yield zinc oxide and water.
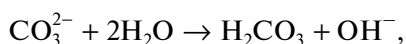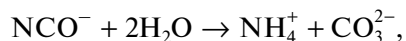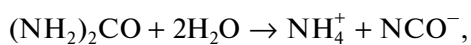
$$NO_3^- + H_2O + 2e^- \rightarrow NO_2^- + 2OH^-,$$

$$Zn^{2+} + 2OH^- \rightarrow Zn(OH)_2,$$

$$Zn(OH)_2 \rightarrow ZnO + H_2O.$$
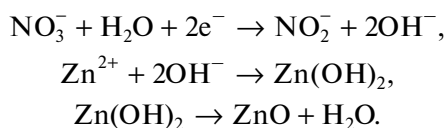
Scheme 2. Schematic representation of ZnO and $Zn_{1-x}Ag_xO$ thin film synthesis by electrodeposition method on FTO substrate.

Mechanism of Chemical Bath Deposited ZnO and Ag−ZnO Thin Films

From the proposed mechanism (Scheme 3), it has been observed that urea in the presence of aqueous solution decomposed into ammonium ions and carbonate ions. These carbonate ions partly hydrolyzed the deionized water to yield OH^- ions that were responsible to increase the pH of solution. The anions generated served as a source of nucleation at the surface of substrate. Maintaining the pH from 6−6.5 to 4.0 controls the precipitation of zinc carbonate hydroxide precipitation. Moreover, at elevated temperatures in urea solution, the decomposition rapidly

occurs up to pH 8.0 allowing the moderate changes in the solution medium which gets constant at pH 9.0 [28].

$$(NH_2)_2CO + 2H_2O \rightarrow NH_4^+ + NCO^-,$$

$$NCO^- + 2H_2O \rightarrow NH_4^+ + CO_3^{2-},$$

$$CO_3^{2-} + 2H_2O \rightarrow H_2CO_3 + OH^-,$$

$$5Zn^{2+} + 2CO_3^{2-} + 6OH^- \rightarrow Zn_5(CO_3)_2(OH)_6.$$

Scheme 3. Schematic representation of ZnO and $Zn_{1-x}Ag_xO$ thin film synthesis by chemical bath deposition method on FTO substrate.

As the sol−gel process involves polycondensation route of molecular precursors in the liquid medium, these particles are then converted into colloids which undergoes agglomeration and sedimentation to form gels. The small oxo-ions so formed during hydrolysis come in competition with the monoacetate ions which act as a nucleophile to form the metal complexes [5, 6].

In the case of chemical bath deposition method, the basic principle lies in the precipitation of solid phase out of solution as a result of super saturation in the chemical bath. So for precipitation to occur, the ions must react on the substrate surface and not in the solution. Moreover, for the complete ion saturation of the precipitation, a complexing agent is required in small amount, which ensures a slow release of ions in the solution. Here urea served as a complexing agent and the source of the ammonium ions and carbonate ions which in turn regulated the pH of the medium as well as provided the nucleation centers at the substrate surface. Thus, chemical bath deposition method follows a controlled chemical kinetics for the synthesis of thin films through the precipitation method that results a solid phase out of solution medium [10] whereas in the sol−gel deposition method, the conversion of monomers results in a colloidal solution that in turn acts as a precursor for the formation of integrated network of the gel on the substrate.

The underlying principle in the electrodeposition method is simply a surface coating methodology. The deposition of an adherent layer of one metal on the substrate surface involves the reduction of ions from the aqueous phase. The nitrate ions from the precursor undergo reduction to yield hydroxyl species. The hydroxide species are formed when the oxygen molecules in the electrolyte gain two electrons which then reacts with Zn^{2+} to form $Zn(OH)_2$. Finally the $Zn(OH)_2$ are dehydrated to ZnO and H_2O at higher temperature (70°C). Moreover, a potential higher than −1.1 V alters the film towards less uniformity [38]. This metal solution interface is considered as the locus of the deposition process. The carriers at the interface accumulate at the boundary and interface acts as a barrier to the flow of charges. The charge carriers in the bulk of two types of phases of interfaces are under the impact of isotropic forces. In the metal−electro-lyte interface, formed after doping, the arrangement of solvent dipoles and ions gets change as a result of these anisotropic forces. Initially, as the charge carriers build up on the two sides of interface, the electrical forces overpower the barrier and results in the flow of charges and the flow stops when the electrochemical potential on the two sides of interface gets equal [7, 9].

On contrary to the sol−gel and chemical bath deposition method, the electrodeposition method offers a controlled departure from equilibrium through the applied potential with the advantage of precise control over the shape and growth mechanisms. All the three methods are solution based and relatively simple but chemical bath and electrodeposition can be processed at low temperatures as well. For the sol−gel deposition method, the coating process is somewhat extensive in terms of formation of colloidal particles following hydrolysis, which then proceeds to polymerization, condensation gelation, ageing and the drying on the conductive substrate. Additionally, for the case of noble metals, which require careful dopant and metal oxide interaction at the charge carrier and surface defects levels, small number of dipping's usually result in the more discrete structures as compared to the electrodeposition.

CONCLUSIONS

Silver doped ZnO films were deposited on FTO substrate at low temperature by sol−gel, electrodeposition, and chemical bath deposition methods. The obtained XRD patterns indicated the presence of hexagonal wurtzite ZnO structure as the sole crystalline quality with all the films oriented along the (101) plane and Ag^+ residing at Zn^{2+} site. The UV−Vis spectroscopic data indicated the decrease in the ZnO band gap (3.2 eV) with the increase in silver content particularly for the films by chemical bath deposition method which indicated the presence of higher number of donor states near the conduction band. The spectroscopic data used for band gap calculations showed that there is a red shift in band gaps with the increase in the silver content, and the increase is more prominent in the electrodeposition and chemical bath deposition methods due to increased compressive strains induced in their crystal structures, e.g., for 3.0 wt % Ag/ZnO thin films, the decrease in the band gap is observed to be 3.21, 3.12, 1.98 eV, respectively. The obtained microstructures from SEM showed increase in aggregation and the film compactness with the increase in silver content except for the sol−gel films where the compact pellet type structures have been transformed into the core shell structures with higher porosity level. Strong evidence for the Ag^+ substitution for the Zn^{2+} sites instead of "O" has been obtained from the SEM images and the EDX data of the pure and doped samples where the oxygen content has almost remained same as compared to that of Zn

content. Overall, the 1.0 wt % Ag doped ZnO thin films showed maximum particle size reduction.

ACKNOWLEDGMENTS

CONFLICT OF INTEREST

The authors declare that they have no conflicts of interest.

SUPPLEMENTARY INFORMATION

The online version contains supplementary material available at https://doi.org/10.1134/S0036024422140217

REFERENCES

1. Z. L. Wang, J. Phys.: Condens. Matter **16**, R829 (2004).

2. A. Janotti and C. G. van de Walle, Rep. Prog. Phys. **72**, 126501 (2009).

3. Q. Zhang, C. S. Dandeneau, X. Zhou, and G. Cao, Adv. Mater. **21**, 4087 (2009).

4. H. Abdullah, A. Omar, M. A. Yarmo, et al., J. Mater. Sci.: Mater. Electron. **24**, 3603 (2013).

5. M. Vaseem, A. Umar, and Y.-B. Hahn, *Metal Oxide Nanostructures and Their Applications* (Am. Sci. Publ., New York, 2010).

6. L. Znaidi, Mater. Sci. Eng., B **174**, 18 (2010).

7. M. Paunovic and M. Schlesinger, *Fundamentals of Electrochemical Deposition* (Wiley, Chichester, 2006).

8. M. Laurenti and V. Cauda, J. Coating **8** (2), 67 (2018).

9. A. J. Bard and L. R. Faulkner, *Electrochemical Methods: Fundamentals and Applications* (Wiley, New York, 2001).

10. A. Kathalingam, N. Ambika, M. Kim, J. Elanchezhiyan, Y. Chae, and J. Rhee, Mater. Sci.-Pol. **28**, 513 (2010).

11. S.-H. Nam, S.-J. Cho, and J.-H. Boo, Nanoscale Res. Lett. **7**, 1 (2012).

12. A. Kuznetsov, Y. Lu, S. Turner, et al., Opt. Mater. Express **2**, 723 (2012).

13. M. Karyaoui, A. Mhamdi, H. Kaouach, et al., Mater. Sci. Semicond. Process. **30**, 255 (2015).

14. H. Atwater and A. Polman, Nat. Mater. **9**, 205 (2010).

15. B. Sebo, N. Huang, Y. Liu, et al., Electrochim. Acta **112**, 458 (2013).

16. L. Xu, J. Miao, Y. Chen, et al., Optik **170**, 484 (2018).

17. T. Touam, F. Boudjouan, A. Chelouche, et al., Optik **126**, 5548 (2015).

18. S. Boulahlib, K. Dib, M. Özacar, and Y. Bessekhouad, Opt. Mater. **113**, 110889 (2021).

19. K. Khojier, Mater. Sci. Semicond. Process. **121**, 105283 (2021).

20. G. Bagha, M. R. Mersagh, H. Naffakh-Moosavy, and L. F. Matin, Ceram. Int. (2021).

21. M. Hjiri, M. Aida, O. Lemine, and L. El Mir, Mater. Sci. Semicond. Process. **89**, 149 (2019).

22. M. Pérez-González and S. Tomás, Catal. Today **360**, 129 (2021).

23. S. Thaowonkaew, M. Kumar, and A. Vora-Ud, J. Electron. Mater., 1 (2021).

24. L. Cui, G.-G. Wang, H.-Y. Zhang, et al., Ceram. Int. **39**, 3261 (2013).

25. M. Lanjewar and J. V. Gohel, Inorg. Nano-Met. Chem. **47**, 1090 (2017).

26. S. M. Ali, W. Farooq, M. Baig, et al., Mater. Sci.-Pol. **33**, 601 (2015).

27. A. Kathalingam, M. Kim, Y. Chae, et al., J. Korean Phys. Soc. **55**, 2476 (2009).

28. H. Abdullah, N. Ariyanto, S. Shaari, et al., Am. J. Eng. Appl. Sci. **2**, 236 (2009).

29. H. Khallaf, G. Chai, O. Lupan, et al., J. Phys. D: Appl. Phys. **42**, 135304 (2009).

30. N. Tarwal and P. Patil, Electrochim. Acta **56**, 6510 (2011).

31. N. Winkler, S. Edinger, W. Kautek, and T. Dimopoulos, J. Mater. Sci. **53**, 5159 (2018).

32. S. Jeong, B. Park, S. Lee, and J.-H. Boo, Surf. Coat. Technol. **193**, 340 (2005).

33. F. Xian, K. Miao, X. Bai, et al., Optik **124**, 4876 (2013).

34. H. Sutanto, S. Wibowo, I. Nurhasanah, and E. Hidayanto, AIP Conf. Proc. **1755**, 150001 (2016).

35. M. Habibi and M. Khaledi Sardashti, Int. J. Nanosci. Nanotechnol. **4**, 13 (2008).

36. H. Rahal, R. Kihal, A. M. Affoune, et al., J. Semicond. **38**, 053002 (2017).

37. D. Chu, T. Hamada, K. Kato, and Y. Masuda, Phys. Status Solidi **206**, 718 (2009).

38. J. Ao, R. Fu, M.-J. Jeng, et al., Materials **11**, 953 (2018).